# A Wide-Band, Wide-Swing Current Driver for Electrical Impedance Tomography Applications

Mohsen Shahghasemi, Kofi M. Odame
*Thayer School of Engineering, Dartmouth College*
*Hanover, New Hampshire, United States of America*
Email: {mohsen.shahghasemi.th, kofi.m.odame}@dartmouth.edu

***Abstract*—A current driver for electrical impedance tomography (EIT) is presented. The current driver is based on a differential input current-conveyor architecture with a wide-swing cascode output stage and a fast-settling servo loop for setting the DC output voltage. The circuit was designed and fabricated as an application specific integrated circuit (ASIC) in a standard CMOS 0.18-$\mu$m technology, uses a 3.3 V single supply voltage, and consumes 13 mW power. It operates from 10 kHz to 40 MHz, providing up to 2.7 $\mathrm{mA_{PP}}$ current with an output voltage compliance of 1.6 $\mathrm{V_{PP}}$, while providing a low frequency output impedance of 315 k$\Omega$ and a total harmonic distortion below 1%. These performance specifications make the proposed current driver suitable for high frequency, high signal-to-noise-ratio (SNR) EIT applications, like detecting cancerous lesions in the prostate tissue.**

***Index Terms*—Current Driver, Electrical Impedance Tomography (EIT)**

## I. Introduction

Electrical impedance tomography (EIT) is a promising imaging technology for improving prostate cancer diagnosis [1]. To form an EIT image, current is injected into the tissue under test, and the resulting voltages on the tissue surface are measured [2], [3], and [4]. A tomography-like impedance map of the tissue can be reconstructed from the injected current and measured voltages [5]; cancerous lesion is identifiable by its higher impedance relative to benign tissue [6]. The advantages of EIT are that it is non-ionizing, inexpensive, and miniaturizable. The challenge is that EIT requires high performance analog components. For instance, the current driver must produce a sinusoidal current with less than 1% total harmonic distortion (THD), operate over a 10 MHz bandwidth, provide up to hundreds of k$\Omega$ of low frequency output impedance, and drive loads up to 7 k$\Omega$.

To date, no current driver has been reported that meets the aforementioned specifications for EIT. The structures proposed in [7] and [8] use a feedback scheme that limits the bandwidth as well as the ability to drive large impedance. In [9], the pulse width modulated (PWM) approach can drive higher loads, but it is only suitable for injection frequencies lower than 1 MHz. Also, none of the aforementioned current drivers was designed to drive a DC-blocking capacitor, which is necessary for patient safety [1]. We recently introduced a current driver that can drive a 10 $\mu$F DC-blocking capacitor, but it provides very low frame rate, and induces an offset on measured voltages due to poor phase margin and slow settling behavior [1]. This paper proposes a current driver that can drive loads up to 7 k$\Omega$ via a DC-blocking capacitor, operate from 10 kHz to 40 MHz and maintain a THD of 1 % while providing fast settling between measurements and a frame rate of 21 frames per second (FPS).

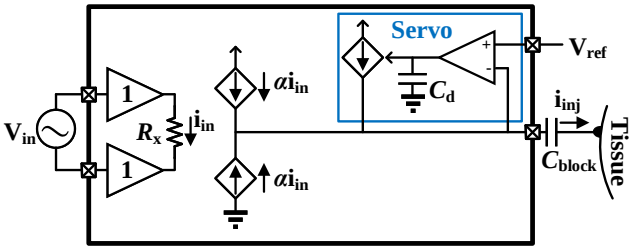


Fig. 1: Top level view of the single-ended current-conveyor based current driver.

## II. Overview of the Solution

Figure 1 depicts the top level view of the proposed current-conveyor-based current driver. The sinusoidal input voltage, $\mathrm{V_{in}}$ is buffered across the resistor $R_\mathrm{x}$ the voltage converts into current via the transconductance $\alpha$ and is injected into the tissue via a DC-blocking capacitor $C_\mathrm{block}$. The poles of the servo loop are designed to allow fast settling of the output DC voltage, with minimal interference with the current driver behavior throughout the bandwidth.

## III. Details of the Solution

The current-conveyor structure is known for its robustness, high linearity, and high swing [10]. Figure 2 shows the transistor level implementation of the proposed current-conveyor based current driver. The flipped source-followers ($\mathrm{M_{1a-5a}}$ and $\mathrm{M_{1b-5b}}$) in the transconductance stage act as a near-unity-gain buffer and apply the input voltage to $R_\mathrm{x}$. The current passing by $R_\mathrm{x}$ is produced through $\mathrm{M_{2a,b}}$ and is then mirrored to $\mathrm{M_{22a,b}}$ in the output stage. The DC servo loop prevents the high-impedance output node from saturating to the power rails. We implemented the DC servo loop as a simple OTA-C integrator (transistors $\mathrm{M_{s0-4}}$ and capacitor $C_\mathrm{d}$) and a tunable current source, $\mathrm{M_{s5}}$. $\mathrm{M_{s6}}$ is used for sinking the current passing through $\mathrm{M_{s5}}$ to make sure there is no systematic change to the current passing through $\mathrm{M_{8b}}$ to $\mathrm{M_{22b}}$.

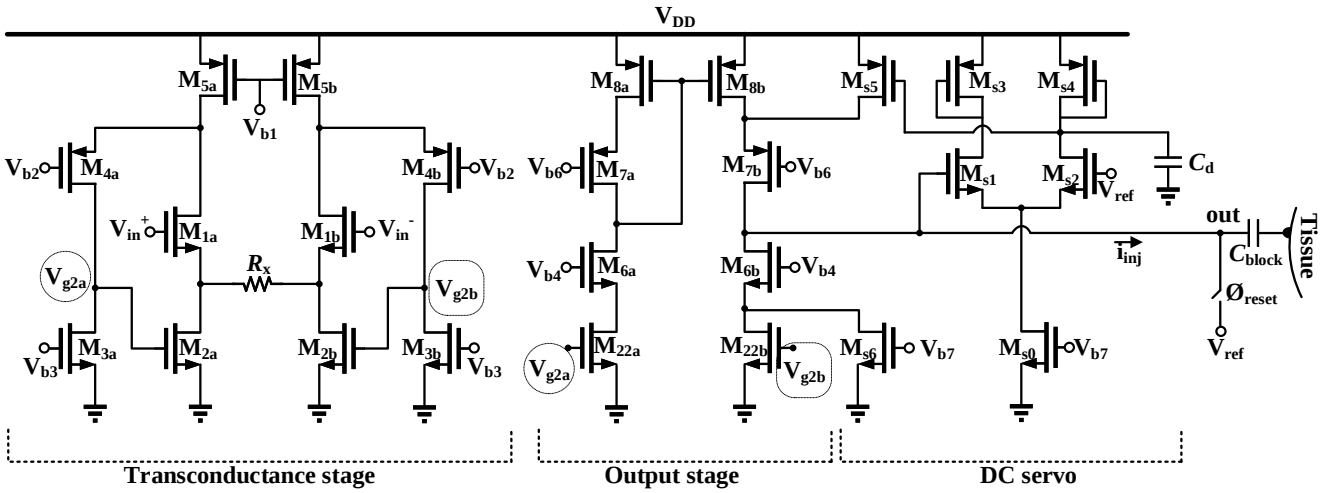


Fig. 2: Transistor level implementation of the single-ended current-conveyor based current driver.

This sets the output DC level to $V_{\rm ref}$ minus some small offset, $V_{\rm err}$, due to the gain and offset of the OTA.

The current driver can be disabled by closing the $\phi_{\rm reset}$ switch, which clamps the output voltage to $\rm V_{ref}$. Operation can be resumed by opening the $\phi_{\rm reset}$ switch, which allows the output voltage to accommodate injected AC current, while the servo loop drives the DC output voltage to ($\rm V_{ref}$ - $\rm V_{err}$). As the current driver switches from disabled to operational, the output voltage will take some finite amount of *settling time* to transition from $\rm V_{ref}$ to ($\rm V_{ref}$ - $\rm V_{err}$). This settling time can be minimized by carefully considering the circuit's main poles and zeros:

$$\omega_{\rm p1} = -\frac{1}{(R_{\rm out} + R_{\rm tissue})C_{\rm block}} \tag{1}$$

$$\omega_{\rm z1} = -\frac{1}{R_{\rm tissue}.C_{\rm block}} \tag{2}$$

$$\omega_{\rm p2} = -\frac{g_{\rm ms4}}{C_{\rm d}} \tag{3}$$

in which, $R_{\rm tissue}$ stands for the tissue resistance and $R_{\rm out}$ denotes the output resistance of the current driver neglecting the high drain-source resistance of $\rm M_{s5,s6}$:

$$R_{\rm out} = g_{\rm m7b}.r_{\rm ds7b}.r_{\rm ds8b}||g_{\rm m6b}.r_{\rm ds6b}.r_{\rm ds22b}. \tag{4}$$

$R_{\rm tissue}$ in series with $C_{\rm block}$ constitutes one low frequency pole ($\omega_{\rm p1}$) and one low frequency zero ($\omega_{\rm z1}$); a pole followed by a zero is not capable of damping the loop gain and that is why we need the servo loop to contribute the additional pole, $\omega_{\rm p2}$. To ensure both loop stability and damping, the $\omega_{\rm p2}$ should be placed at frequencies higher than ($\omega_{\rm z1}$). Also, $\omega_{\rm p2}$ should be placed below the current driver's operating frequency range (i.e. $<$ 10 kHz).

## IV. Results

The circuit has been designed, simulated, and tested in 0.18 $\mu$m CMOS technology with a 3.3 V supply voltage consuming 13 mW power. Figure 3 shows 200 Monte Carlo simulations of the output of the current driver after $\phi_{\rm reset}$ goes off. Depending on the mismatch , the output can jump at most 350 mV (up or down) and then settle to a voltage in the range of 1.855 V to 1.945 V (3$\sigma$ range). In the worst case of the simulation, the settling error after 0.15 ms is equal to 50 mV which can be filtered out in the digital domain as we are just focused on the AC signals.

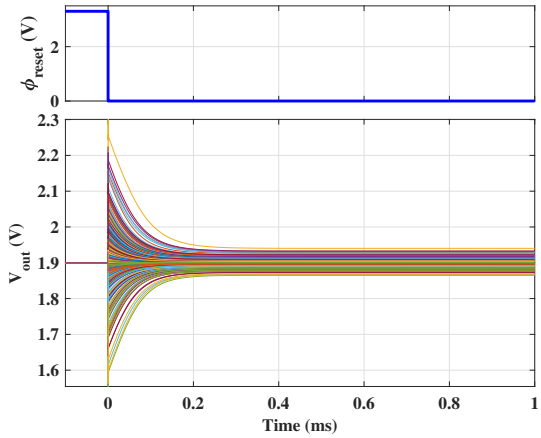


Fig. 3: Settling behavior of the node out of Fig. 2. The $\phi_{\rm reset}$ switch (see Fig. 2) is open at t = 0, and the servo loop adjusts node $\rm V_{out}$ equal to 1.9 V. Plot shows the results of 200 Monte Carlo simulation runs.

Assuming 32 measurement per interrogation frequency and 9 frequencies, we have 288 measurements per frame. Each measurement take roughly 10 $\mu$s. So, with a 0.15 ms settling time between each measurements, the frame rate is 21 FPS.

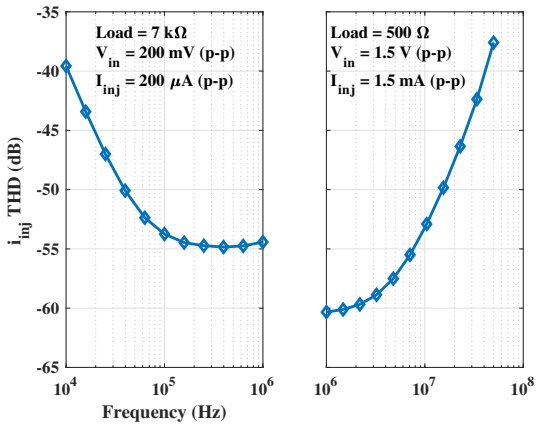


Fig. 4: THD simulation of the current driver for high impedance load at low frequency and low impedance load at high frequency.

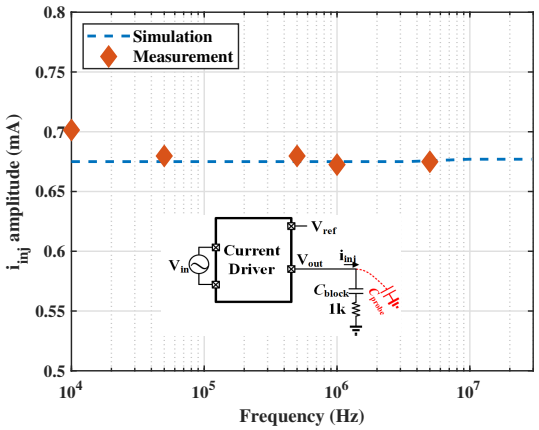


Fig. 6: Measurement results of injected current amplitude versus frequency, for a 1 kΩ load.

This meets the 10 FPS frame rate that is typically required to minimize motion artifact and patient discomfort.

Figure 4 shows the simulated THD of the current driver. Since the tissue impedance changes with the frequency, two different impedance has been used. The system can maintain the THD of 1 % (-40 dB) up to the frequency of 40 MHz. The increase of harmonic distortion at low frequencies is caused by the servo loop since its loop gain is not still negligible.

Figure 5 depicts the simulation results of the output THD vs. input amplitude at the frequency of 10 MHz. The load resistance is chosen to be 600 Ω which is close to the tissue impedance at that frequency. As is seen, the current driver has an acceptable THD while having output voltage amplitudes up to 0.8 V; this is the output compliance of 1.6 $V_{pp}$ leads to 2.7 $mA_{pp}$ maximum output current. For safety reasons, the current should stay below 2 $mA_{pp}$ at 10 kHz [11] and it can go to 2.7 $mA_{pp}$ at higher frequencies. The current also can be limited by the load impedance as the output swing should be lower than the voltage compliance.

A load of 1 kΩ is placed at the output of the current driver and the output current $i_{inj}$ is measured through voltage at node $V_{out}$ using an oscilloscope probe with a parasitic capacitance of 46 pF, shown as $C_{probe}$ in the schematic depicted in Fig. 6. The measurement results and the simulations results with similar load are shown in Fig. 6; the measurement was calibrated with the knowledge that $C_{probe}$ is shunting current. As is seen, the measured injected current is in close agreement with the simulations. Testing at higher frequencies was skipped because of the poor measurement quality.

Figure 7 shows the output impedance versus frequency. A voltage source is applied to the output and the current is measured. The output impedance ranges from 100 kΩ to 315 kΩ at low frequencies and is above 10 kΩ at frequencies higher than 6 MHz; this is sufficient to drive tissue, which presents a load of a few hundred Ohms at these higher frequencies; the output resistance is low at lower frequencies because of the servo loop operations. The die micrograph and the layout are shown in Fig. 8, the current driver block occupies an area of $0.13 \times 0.24$ $mm^2$.

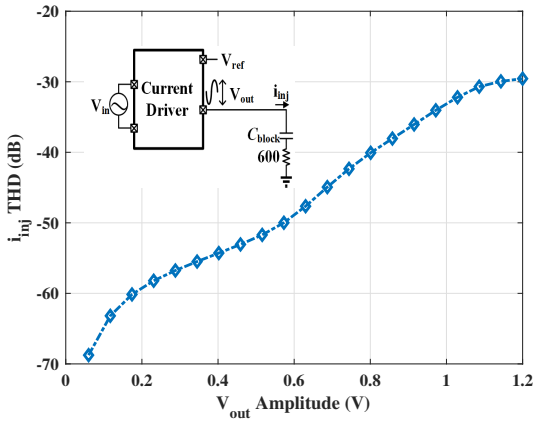


Fig. 5: Simulation of the injected current THD versus output voltage amplitude. Injected current frequency is 10 MHz and load resistance is 600 Ohms.

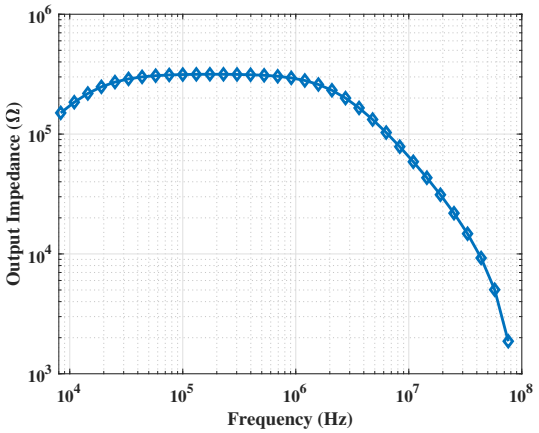


Fig. 7: Simulation of the output impedance of the current driver.

TABLE I: Performance comparison of the state of the art current drivers.

| Parameter | Constantinou *et al* [12] | Hong *et al* [3] | Kim *et al* [7] | Wu *et al* [8] | Rao *et al* [1] | This work* |
|---|---|---|---|---|---|---|
| Architecture | Negative feedback | Differential current generator | Differential current generator | Negative feedback | Current conveyor | Current conveyor |
| Bandwidth | 90 kHz | $\leq$ 200 kHz | 256 kHz | 500 kHz | 100 Hz - 10 MHz | 10 kHz - 40 MHz |
| Output impedance | 360 kΩ @ 1 MHz | —— | —— | 1.12 MΩ @ 500 kHz | 101 kΩ @ 1MHz<br>19.5 kΩ @ 10 MHz | 100 kΩ @ 10 kHz<br>300 kΩ @ 1 MHz<br>10 kΩ @ 40 MHz |
| Maximum output current (peak-peak) | 1 mA | 1 mA | 1 mA | 6 mA | 1.2 mA | 2.7 mA |
| THD (current) (frequency) | $<$ 0.1 % (1 mA) (50 kHz) | $<$ 0.1 % (0.1 mA) (Unknown) | $<$ 0.47 % (1 mA) (128 kHz) | $<$ 0.18 % (6 mA) (500 kHz) | $<$ 0.14 % (1.2 mA) (500 kHz)<br>$<$ 0.7 % (1.2 mA) (10 MHz) | $<$ 1 % (1.5 mA) (40 MHz) |
| Voltage compliance (Peak-peak) | 4 V | 0.4 V | —— | 14 V | 0.6 V | 1.6 V |
| Settling time | Unknown | Unknown | Unknown | Unknown | 25 s | 0.15 ms |

* Simulation Results

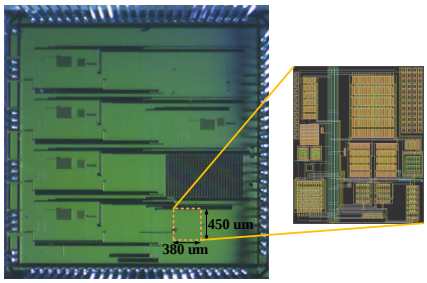


Fig. 8: The die micrograph and the layout of the current driver.

## V. Discussion

The proposed circuit can increase the frame rate considerably compared to [1] and is capable of accommodating larger output swings. Table I compares this work with multiple state-of-the-art designs. The proposed current driver exhibits a wide operating bandwidth, and an output impedance that is suitable for prostate cancer imaging. The THD is within the acceptable range up to very high frequencies based on the simulations.

## VI. Conclusion

A current driver has been designed to drive loads up to 7 kΩ over the frequency range of 10 kHz to 40 MHz. It includes a DC servo-loop that allows the current driver to drive a 10 $\mu$F DC blocking capacitor (for patient safety), while providing a fast settling time of 0.15 ms. The current driver was designed, simulated and measured in a 0.18 $\mu$m CMOS technology.

## VII. Acknowledgments

This work was supported in part by the U.S. National Science Foundation, under Grant No. 1418497, U.S. DoD CDMRP Grant No s. W81XWH-15-1-0572 and W81XWH-15-1-0571.

## References

[1] A. J. Rao, E. K. Murphy, M. Shahghasemi, and K. M. Odame, "Current conveyor based wide-band current driver for electrical impedance tomography," *Physiological measurement*, 2019.

[2] R. J. Halter, A. Hartov, and K. D. Paulsen, "A broadband high-frequency electrical impedance tomography system for breast imaging," *IEEE Transactions on biomedical engineering*, vol. 55, no. 2, pp. 650–659, 2008.

[3] S. Hong, J. Lee, J. Bae, and H.-J. Yoo, "A 10.4 mw electrical impedance tomography soc for portable real-time lung ventilation monitoring system," *IEEE Journal of Solid-State Circuits*, vol. 50, no. 11, pp. 2501–2512, 2015.

[4] R. Bayford and A. Tizzard, "Bioimpedance imaging: an overview of potential clinical applications," *Analyst*, vol. 137, no. 20, pp. 4635–4643, 2012.

[5] E. K. Murphy, M. Takhti, J. Skinner, R. J. Halter, and K. Odame, "Signal-to-noise ratio analysis of a phase-sensitive voltmeter for electrical impedance tomography," *IEEE transactions on biomedical circuits and systems*, vol. 11, no. 2, pp. 360–369, 2016.

[6] J. Jossinet, "The impedivity of freshly excised human breast tissue," *Physiological measurement*, vol. 19, no. 1, p. 61, 1998.

[7] M. Kim, J. Jang, H. Kim, J. Lee, J. Lee, J. Lee, K.-R. Lee, K. Kim, Y. Lee, K. J. Lee *et al.*, "A 1.4-m$\Omega$-sensitivity 94-db dynamic-range electrical impedance tomography soc and 48-channel hub-soc for 3-d lung ventilation monitoring system," *IEEE Journal of Solid-State Circuits*, vol. 52, no. 11, pp. 2829–2842, 2017.

[8] Y. Wu, D. Jiang, A. Bardill, S. de Gelidi, R. Bayford, and A. Demosthenous, "A high frame rate wearable eit system using active electrode asics for lung respiration and heart rate monitoring," *IEEE Transactions on Circuits and Systems I: Regular Papers*, no. 99, pp. 1–11, 2018.

[9] Y. Wu, D. Jiang, P. Langlois, R. Bayford, and A. Demosthenous, "A power-efficient current generator with common mode signal autozero feedback for bioimpedance measurement applications," in *2019 IEEE International Symposium on Circuits and Systems (ISCAS)*. IEEE, 2019, pp. 1–4.

[10] A. Sedra and K. Smith, "A second-generation current conveyor and its applications," *IEEE Transactions on circuit theory*, vol. 17, no. 1, pp. 132–134, 1970.

[11] W. R. Lionheart, J. Kaipio, and C. N. McLeod, "Generalized optimal current patterns and electrical safety in eit," *Physiological measurement*, vol. 22, no. 1, p. 85, 2001.

[12] L. Constantinou, R. Bayford, and A. Demosthenous, "A wideband low-distortion cmos current driver for tissue impedance analysis," *IEEE Transactions on Circuits and Systems II: Express Briefs*, vol. 62, no. 2, pp. 154–158, 2015.